

# Non-isothermal crystallisation kinetics with instantaneous nucleation

J.A. Martins<sup>a,\*</sup>, J.J.C. Cruz Pinto<sup>b</sup>

<sup>a</sup>*Departamento de Engenharia de Polímeros, Universidade do Minho, Campus de Azurém, 4800 Guimarães, Portugal*

<sup>b</sup>*Departamento de Química, Universidade de Aveiro, 3810, Aveiro, Portugal*

Received 14 May 1999; accepted 10 January 2000

---

## Abstract

The problem of the kinetics of non-isothermal crystallisation is analysed both from a theoretical and experimental point of view. The most common equations used to describe the kinetics of non-isothermal crystallisation—the Nakamura and Ozawa equations—are analysed and discussed. The Nakamura equation is re-derived without invoking the isokinetic condition, and it is shown that this equation is valid only for non-isothermal crystallisation with instantaneous nucleation. It is also shown that the Ozawa equation for pre-determined nucleation is incorrect. A Tobin-type equation for non-isothermal crystallisation with instantaneous nucleation is also derived. The experimental problems related with the recording of data for this type of crystallisation are also analysed and discussed. As a further test of the validity of the theoretical models, and as a justification for the use of isothermal crystallisation data to model non-isothermal processes, the (time-dependent) real sample temperature increase in nominally isothermal experiments was quantified. The isothermal process was then treated as a truly non-isothermal one, from the (low thermal conductivity) sample's standpoint. © 2000 Elsevier Science Ltd. All rights reserved.

*Keywords:* Crystallisation; Non-isothermal; Modelling

---

## 1. Introduction

The practical importance of an accurate description of the kinetics of non-isothermal crystallisation has been already stressed in the literature published on this subject [1]. Several models and modifications have been published [1–3]. Among the most used and applied are the Nakamura [4–6] and Ozawa equations [7].

The Nakamura equation is a modification of the Komolgorrof [8]–Avrami [9–11]–Evans [12] equations for isothermal crystallisation. In order to apply Avrami's equation to non-isothermal crystallisation kinetics, Nakamura makes use of the “isokinetic” assumption. The basic idea of this assumption is to allow the extension of the Avrami equation for sporadic nucleation to non-isothermal conditions. According to the author, Nakamura's equation is valid only within a temperature range where the ratio between the secondary nucleation growth rate ( $G(T)$ ) and the activation frequency of primary nuclei have the same temperature dependence, i.e. their ratio is constant. For instantaneous nucleation, the activation frequency is infinite and therefore the isokinetic assumption is unnecessary and

meaningless. For sporadic nucleation, the assumption is valid only in the earlier stages of the crystallisation process and the final equation then obtained is identical to that for instantaneous nucleation. Below, Nakamura's equation is derived without the isokinetic assumption, and it is shown that the equation is only valid for non-isothermal crystallisation with instantaneous nucleation. A Tobin-type equation for non-isothermal crystallisation is also derived.

Concerning the use of these equations, they are generally expressed as a transformed mass fraction as a function of time, instead of temperature—the natural variable for non-isothermal crystallisation. The time is usually set to zero at the temperature at which the start of the exothermal process is detected by the device [14,15]. Instead, it should be set at the time where the thermodynamic or other material's characteristic melting temperature is reached. The first one is determined using the standard Hoffman–Weeks plots. Since some uncertainty might be associated with this temperature, a material's melting temperature may be determined experimentally. For this purpose, the experimental procedure uses first a slow cooling (at 0.1 K/min) followed by melting also at a low scanning rate, with the instrument adequately calibrated at that same scanning rate.

Using a reasoning similar to that used by Evans (also followed later by Nakamura), Ozawa [7] derived equations for non-isothermal crystallisation with instantaneous and

---

\* Corresponding author. Tel.: + 351-253-510245; fax: + 351-253-510249.

*E-mail addresses:* zmartins@eng.uminho.pt (J.A. Martins), cpinto@dq.ua.pt (J.J.C. Cruz Pinto).

sporadic nucleation. Comments on the validity of both Ozawa equations are made below.

In addition to theoretical considerations concerning the applicability of the Nakamura and Ozawa equations, some experimental considerations are indeed important and often forgotten. The first one, accounted for by most workers, is related to the determination of the sample's thermal resistance and the evaluation of its effect on the true sample temperature. The second one is related to the calibration on cooling of the DSC. It is generally (even if not explicitly) assumed that the standard calibration performed on heating is also valid for cooling experiments, but the temperature (or time) scale may in fact be affected by large deviations [16,17].

Further, in order to ascertain the validity of the theoretical models, namely Nakamura's and Tobin's equations, they will also be used with isothermal crystallisation data, to evaluate the effect of the sample temperature rise due to the heat released during crystallisation.

## 2. Theory

### 2.1. The Nakamura equation

The procedure used here to derive the Nakamura equation is different from the original one [17].

Considering the nomenclature used by different authors, it is important to define some important concepts pertaining to primary nucleation. The nomenclature followed is that used by Wunderlich [18, Section 5.1.5]. Instantaneous (or athermal) nucleation implies that all crystals start growing at the same time. This kind of nucleation is sometimes indistinctly named heterogeneous or pre-determined. In fact, this last form of nucleation can be instantaneous (athermal) or sporadic (thermal). In this work, only the instantaneous (or athermal) nucleation will be treated. The case of sporadic nucleation will be treated elsewhere [19].

Let us consider, like in isothermal crystallisation, that  $\bar{N}$  is the mean number of potential nuclei existing in a unit volume of untransformed material. For freely growing spheres, the mass fraction transformed between  $t$  and  $t + dt$  is

$$dX' = \frac{\rho_s}{\rho_l} \bar{N} 4\pi r^2 dr, \quad (1)$$

with  $r = Gt$ , where  $G$  is the linear growth rate of the spheres and  $r$  their radius at time  $t$ . The above equation may be written as:

$$dX' = \frac{\rho_s}{\rho_l} \bar{N} 4\pi r^2 G dt = \frac{\rho_s}{\rho_l} \bar{N} 4\pi r^2 G \frac{dt}{dT} dT, \quad (2)$$

where  $dT/dt = \dot{T}$ , is the scanning rate—negative for a cooling scan;  $\rho_s$  and  $\rho_l$  are the solid and liquid phase densities.

The impingement effect between growth fronts is accounted for by Avrami as

$$dX(T) = [1 - X(T)] dX'(T), \quad (3)$$

where  $dX(T)$  is the effective differential increment of the mass fraction of material transformed to the new (solid, semi-crystalline) phase. From Eqs. (2) and (3), we have

$$\int_0^X \frac{dX}{1-X} = \frac{4\pi\rho_s\bar{N}}{\rho_l} \int_{T_m^0}^T \frac{r^2 G(T')}{\dot{T}} dT'. \quad (4)$$

On the left-hand side of Eq. (4), the integral limits are set to zero and  $X$ , respectively, at the start of the crystallisation process and at the current temperature  $T$ . The lower limit of the integral in the right-hand side is the thermodynamic melting temperature, i.e. the exact temperature at which the crystallisation process may effectively start with probability  $\geq 0$ .

To solve the integral in Eq. (4), it is necessary to express the radius  $r$  as a function of known variables. Since  $r$  is related to the linear growth rate of the spheres, it is possible to write the relation:

$$r(t) = \int_0^t G(T) dt = \int_{T_m^0}^T G(T') \frac{1}{\dot{T}} dT' = \frac{T - T_m^0}{\dot{T}} \bar{G}(T), \quad (5)$$

where  $\bar{G}(T)$  is the mean value of the linear growth rate between  $T$  and  $T_m^0$ . The last equality, however, is valid when (and only when) the temperature scanning rate is constant.

The introduction of Eqs. (5) into (4) and the solution by parts of the integral in the right-hand side of this last equation give

$$\int_{T_m^0}^T \frac{r^2 G(T')}{\dot{T}} dT' = r^2 \int_{T_m^0}^T \frac{G(T')}{\dot{T}} dT' - 2 \int_{T_m^0}^T \frac{G(T')}{\dot{T}} \times \left[ \int_{T_m^0}^{T'} \frac{G(T'')}{\dot{T}} dT'' \right]^2 dT' = \frac{r^3}{3}. \quad (6)$$

With the above result, the solution of Eq. (4) is

$$-\ln[1 - X(T)] = \frac{4\pi\rho_s\bar{N}}{3\rho_l\dot{T}^3} [\bar{G}(T)]^3 (T - T_m^0)^3, \quad (7)$$

for constant scanning rate, which is the Nakamura–Avrami equation for non-isothermal crystallisation with instantaneous nucleation, but its general form is

$$X(T) = 1 - \exp\left\{-\left[\int_{T_m^0}^T Z(T') \frac{1}{\dot{T}} dT'\right]^n\right\}, \quad (8)$$

valid even if  $\dot{T}$  is not constant, where  $n$  is the Avrami index, with exactly the same physical meaning as the exponent used in isothermal crystallisation kinetics.  $Z(T) = [K(T)]^{1/n}$ , where  $K(T)$  is the kinetic constant of the Avrami equation. For instantaneous nucleation of spheres,  $n$  is 3 and

$$K(T) = \frac{4\pi\rho_s\bar{N}}{3\rho_l} [G(T)]^3. \quad (9)$$

All parameters in the above equations have their usual meanings. In the transport factor of  $G(T)$ , both the activation energy ( $U^*$ ) and the temperature at which the molecular mobility ceases ( $T_\infty$ ) may play important roles, particularly

in the crystallisation of some slowly crystallising polymers. It is common practice to write the above factor with a WLF functionality, i.e.

$$\exp\left(-\frac{U^*}{R(T' - T_\infty)}\right) = \exp\left(-\frac{C_1 C_2}{C_2 + T' - T_g}\right),$$

where  $C_1$  and  $C_2$  are constants [20].

## 2.2. The Ozawa equation for pre-determined nucleation

According to Ozawa, and using Evans' formalism, the mean number of growth fronts that arrive at an arbitrary point in the melt, for pre-determined nucleation and free growth of spherical nuclei, is Eq. (18) of Ref. [7],

$$\lambda(T) = \pi \bar{N} \int_{T_m^0}^T r^2 dr. \quad (10)$$

Instead, this number should of course be larger by a factor of 4, surely at least for instantaneous nucleation, i.e.

$$\lambda(T) = 4\pi \bar{N} \int_{T_m^0}^T r^2 dr. \quad (11)$$

For constant cooling rate, the radius of the sphere at time  $t$  is given by Eq. (2) of Ref. [7],

$$r(t) = \int_\tau^t G dt = \frac{1}{\dot{T}} \int_\theta^T G(\theta') d\theta' = \frac{1}{\dot{T}} [R(T) - R(\theta)], \quad (12)$$

with

$$R(T) = \int_{T_m^0}^T G(\theta) d\theta, \quad (13)$$

where  $T$  is the temperature at the time  $t$ ,  $\theta$  the temperature at the time  $\tau$  and  $T_m^0$  the thermodynamic melting temperature.

Pre-determined nucleation can be instantaneous or sporadic in nature. For instantaneous (athermal) nucleation, all nuclei become active at the start of the crystallisation process. In this way, the lower limit in the integral of Eq. (12) should be set to zero time or at the thermodynamic melting temperature, and not at  $\tau$  and  $\theta$ , respectively. For the case of pre-determined sporadic nucleation (thermal), the activation frequency of the nuclei should be accounted for, and the above procedure does not reflect this fact. It is shown elsewhere that the Ozawa equation for sporadic nucleation is also incorrect [17,19].

When the lower limits in the integrals of Eq. (12) are set to the appropriate values for pre-determined instantaneous nucleation, i.e.  $\tau = 0$  and  $\theta = T_m^0$ , and using Eqs. (12) and (13), Eq. (10) may be written as

$$\lambda(T) = \pi \bar{N} \int_{T_m^0}^T \frac{r^2 G(\theta)}{\dot{T}} d\theta. \quad (14)$$

This is almost exactly the same as Eq. (4)—the Nakamura equation for instantaneous nucleation—the only difference being the factor  $(4\rho_s/\rho_l)$ . The absence of the factor *four* and the *ratio between the solid and the liquid phase densities* in

Eq. (10) introduces an error into the calculation of the surface area of the spherical nuclei. Both quantitatively and from a strictly physical point of view, this is important.

## 2.3. Tobin's equation

The main difference between Tobin's [21,22] and Avrami–Evans' formalisms is the way used to correct for the impingement between the solid crystalline structures. Some of the assumptions on which depends the validity of Avrami's equation were presented by Wunderlich [18], one of which is a constant density of the solid (semi-crystalline) structures, equivalent to assuming that they are compact and strictly impenetrable. There are several ways of rationalising a Tobin-like type of behaviour [23,24], other than the oversimplified original one [21–23], which still remain open to question [25], but many experiments clearly document the possibility of such behaviour [17,23].

In this equation, the effect of the impingement between solid growth fronts is accounted for by

$$X(t) = [1 - X(t)]X'(t), \quad (15)$$

where the mass fraction transformed by free growth of spherical nuclei is

$$X'(t) = \frac{4\pi\rho_s\bar{N}}{\rho_l} \int_{T_m^0}^T \frac{r^2 G(T')}{\dot{T}} dT'. \quad (16)$$

The solution of the last integral by the same procedure used with Eq. (4), followed by substitution in Eq. (15), yields

$$\frac{X(T)}{1 - X(T)} = \frac{4\pi\rho_s\bar{N}}{3\rho_l} \left[ \int_{T_m^0}^T G(T') \frac{1}{\dot{T}} dT' \right]^3, \quad (17)$$

or the general equation

$$\frac{X(T)}{1 - X(T)} = \left[ \int_{T_m^0}^T Z(T') \frac{1}{\dot{T}} dT' \right]^n. \quad (18)$$

The parameters in the above equation have exactly the same meaning as those in the Nakamura equation (8).

Both Nakamura's and Tobin's equations may be applied to describe non-isothermal quiescent crystallisation processes, even when the cooling rate is not constant. It is only needed to evaluate the temperature variation with time, calculate its derivative and perform a variable substitution in the integrals of Eqs. (8) and (18), to change the independent variable from *temperature* to *time*. Further, the parameters used to describe isothermal crystallisation at different temperatures should also be valid for non-isothermal crystallisation.

The procedure for the treatment of non-isothermal results using isothermal data was summarised by Patel [26]. The parameters in Nakamura's and Tobin's equations are the exponent,  $n$ , the activation energy for transport of polymer molecules to the secondary nuclei,  $U^*$ , the temperature at which the molecular mobility ceases,  $T_\infty$ , (or in alternative to  $U^*$  and  $T_\infty$ ,  $C_1$  and  $C_2$ ), the parameter related with the folded and extended chain surface energies of the critical

secondary nuclei,  $K_g$  (here independent of the existence of regime transitions), the pre-exponential factor of the linear growth rate,  $G_o$ , the mean number of primary nuclei,  $\bar{N}$ , and the ratio between the solid and liquid phase densities. According to the theory of Lauritzen and Hoffman a general formula for  $K_g$  is  $K_g = cb\sigma\sigma_e T_m^0 / (K_B \Delta H)$ , where  $c$  is 4 for regimes I and II and 2 for regime II, the other parameters having their usual meaning. From these, the only parameters that cannot be directly determined from experimental crystallisation data are  $\bar{N}$ , the ratio between the densities and the exponent  $n$ . For fast crystallising polymers, also the parameters of the transport term cannot be accurately measured. However, they can be estimated from a non-linear fit of the radial growth rate expression to isothermal spherulite growth data. For modelling purposes,  $\bar{N}$ ,  $\rho_s/\rho_l$  and  $G_o$  may be included in an overall pre-exponential factor to be fitted to the experimental data, and  $K_g$  and  $U^*$  may be determined from isothermal crystallisation data at different temperatures, obtained by DSC (using the half crystallisation time) or polarised optical microscopy [13].

For a specified cooling rate (constant or variable in time), it is possible to fit the Nakamura and Tobin equations (Eqs. (8) and (18)) to non-isothermal data by adjusting only two parameters—an overall pre-exponential constant ( $C$ ) and the exponent ( $n$ ). Accepted universal values for  $C_1$  and  $C_2$  are 25 and 30, respectively.

For some materials, where it is only possible to obtain isothermal crystallisation data in a narrow temperature range,  $K_g$  and  $U^*$  may be affected by large errors. When this is the case, those parameters can also be fitted to the experimental data.

#### 2.4. Description of isothermal crystallisation data with non-isothermal models

In a scan performed in a differential scanning calorimeter, there is always a thermal lag between the temperature read by the temperature sensor and the real sample temperature. The causes of this thermal lag are the oven, aluminium pan and sample thermal resistances. When the sample used is a standard metal, and the DSC is calibrated for a heating experiment at a specified scanning rate, the above thermal lag is automatically corrected for. Another correction automatically performed during the calibration for a heating experiment is the isothermal correction (for zero scanning rate). So, when a sample other than the calibration standard is scanned on heating, the only thermal lag that remains to be corrected is that due to the sample's characteristics, i.e. its thermal resistance, which differs from that of the calibration standard used. For a cooling scan, all the above three corrections need to be carried out [16,17].

In an isothermal or non-isothermal crystallisation experiment, the sample temperature may differ from the temperature read by the temperature sensor by another factor, in addition (but also connected) to the sample thermal resis-

tance. The factor in question is the effect of the heat of crystallisation that is released.

Considering the above factors, the calculation of the true sample temperature during a crystallisation experiment may be done by performing a heat balance, such that the difference between the sample and reference instrument-sensed input heat fluxes is the sensible heat flux received by the sample minus the heat flux released within the sample due to the ongoing crystallisation process [17,27], i.e.

$$m\bar{C}_p \frac{dT_t}{dt} - |\Delta\dot{Q}| = \frac{1}{R_s}(T_m - T_t), \quad (19)$$

where  $m$  is the sample mass,  $\bar{C}_p$  the specific heat capacity,  $dT_t/dt$  the rate of sample temperature variation and  $T_t$  and  $T_m$  are, respectively, the true sample temperature and the temperature measured by the sample temperature sensor. The heat flux released within the sample is  $|\Delta\dot{Q}| = m|\Delta H_c|dX/dt$ , where  $\Delta H_c$  is the heat of crystallisation and  $X$  the mass fraction transformed at time  $t$ . According to Kriegl and co-workers, the additional effect of the specific heat capacity and mass of the aluminium pan should also be considered [28]. Although more correct from a physical point of view, the sample temperature profile obtained with this procedure is the same as that obtained with Eq. (19) [17].

Eq. (19) is a first-order differential equation which can be numerically solved to find the true sample temperature as a function of time simultaneously with the degree of liquid to solid phase conversion. For that, the above equation may be directly applied to the raw data obtained from the DSC,  $\Delta Q(t)$ , relative to the appropriate crystallisation peak baseline, or to the integrated transformed mass fraction data,  $X(t)$ .

### 3. Experimental

All the experiments in this work were performed with a Perkin Elmer DSC-7 in standard mode. Before each scan at a specified scanning rate, both the temperature and enthalpy calibrations were performed. All cooling scans were performed with the DSC temperature calibration used for conventional heating experiments. After the scans, the sample thermal resistance was determined using the standard procedure (see below).

The materials analysed were: POM—Delrin 150 ( $\bar{M}_w = 70\,000$ ,  $T_m^0 = 198.91^\circ\text{C}$ ,  $T_g = -81.4^\circ\text{C}$ ), PEEK—ICI 450G ( $\bar{M}_w = 40\,000$ ,  $T_m^0 = 389.0^\circ\text{C}$ ,  $T_g = 145^\circ\text{C}$ ), MDPE ( $\bar{M}_w \cong 30\,000$ ,  $T_m^0 = 131.48^\circ\text{C}$ ,  $T_g = -81.4^\circ\text{C}$ ), PE (GPC sample standard,  $\bar{M}_w = 32\,100$ ,  $\bar{M}_w/\bar{M}_n = 1.10$ ). The values for the thermodynamic melting temperature were calculated by extrapolation from the experimental values using the Hoffman and Weeks plot construction. Other values were taken from manufacturers' literature or from Refs. [29,30].

Different samples with similar masses were prepared and analysed, in order to evaluate the homogeneity of the

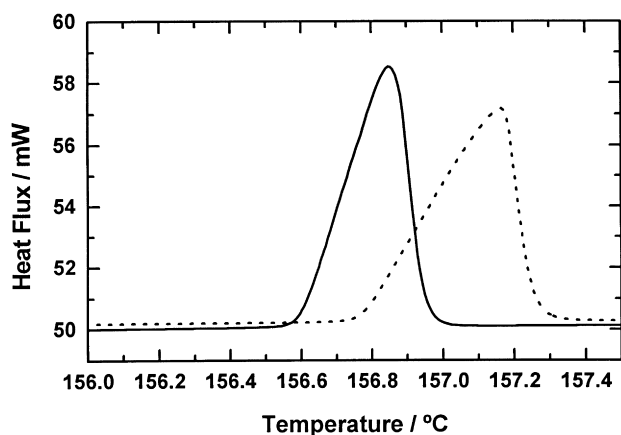


Fig. 1. Measurement of the thermal resistance of a polyoxymethylene sample (thickness = 0.18 mm; area = 13.65 mm<sup>2</sup>; sample mass = 4.197 mg, sample resistance = 24.72 K/W); indium sample (area = 6.95 mm<sup>2</sup>, thickness = 0.08 mm, mass 3.998 mg). Both runs were obtained with the standard temperature calibration on heating at a scanning rate of 1 K/min. Solid line—indium. Dashed line—indium over POM.

materials. Sections of samples crystallised in the DSC at different scanning rates were cut and analysed by polarised optical microscopy, to determine the type of nucleation. As for PEEK, the same grade used in our experiments was analysed by other authors [30], and it was concluded that the nucleation is heterogeneous.

For POM at low scanning rates (less than  $-1$  K/min) the nucleation is predominantly instantaneous, but zones where

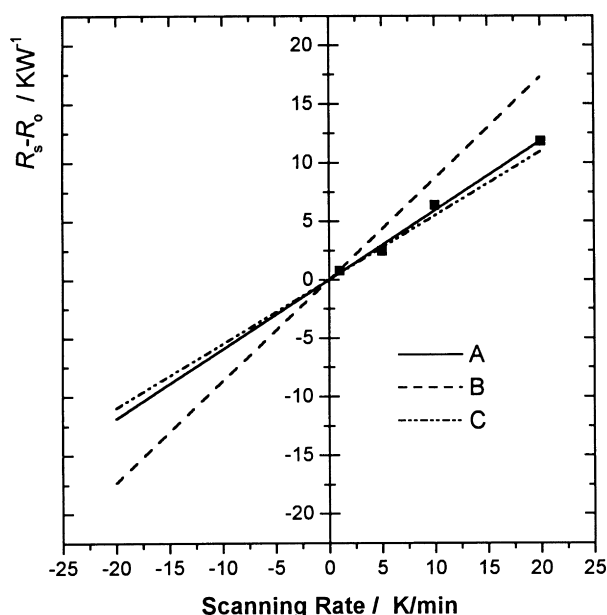


Fig. 2. Variation of the sample's thermal resistance with the scanning rate. The thermal resistances in the ordinate are subtracted from the value extrapolated to zero scanning rate. Curve (A): thermal resistance of the oven, aluminium pan and indium, subtracted by 27.22 K/W. Curve (B): all of curve (A) plus the thermal resistance of MDPE, subtracted by 38.04 K/W. Curve (C): the same as in (B) but for a POM sample, subtracted by 51.94 K/W. The full squares are experimental data for indium.

the boundaries of spherulites are branches of hyperbolae could be identified. For high scanning rates, the nucleation is instantaneous and no traces of sporadic nucleation were found.

For MDPE, it was observed that the nucleation is predominantly instantaneous and that a large number of columnar type structures are formed both at the bottom and top surfaces of the sample, as well as in the bulk. For the PE GPC standard, it was found that the nucleation is mixed, but predominantly instantaneous, for scanning rates lower than  $-1$  K/min, and instantaneous for higher scanning rates.

## 4. Results

### 4.1. Measurements of the sample's thermal resistance

A common procedure to find the sample's thermal resistance is as follows [31]. First, a small amount of indium is placed in an aluminium pan and melted at the scanning rate that will be used in further experiments. The reciprocal of the slope of the ascending peak is the thermal resistance of the oven, aluminium pan and indium sample. Next, a polymer sample with a mass similar to the one that will be analysed (ideally, exactly the same sample) is flattened to fit a similar aluminium pan. The indium sample is carefully taken off from the pan, placed at the top of the polymer sample, and gently pressed against it; the pan is then sealed and a new scan carried out. The result of the above experiment over a sample of POM is shown in Fig. 1. The slope of the ascending part of this new indium peak is different from the first one as well as the onset. The difference between the reciprocal of the slopes of the two indium peaks is the polymer sample's thermal resistance, which depends mainly on its mass and shape.

Similar experiments were also performed for other samples used. As an example, Fig. 2 shows the results for indium and indium over MDPE and POM samples, at scanning rates from 1 up to 20 K/min. In all of these curves, and in order to show the scanning rate dependence of the values of the thermal resistances, they are subtracted of the extrapolated values of the sample's thermal resistance at zero scanning rate. The results for cooling scans are extrapolated from the heating scans. A similar behaviour to the one shown in Fig. 2 was recently found by Richardson for sapphire discs [32].

The extrapolated zero scanning rate value for indium is 27.22 K/W, which is close to the value indicated by the instrument's manufacturer for the *thermal resistance of the DSC oven and sensors* (30 K/W). The thermal resistance of indium itself is small in comparison with the other thermal resistances involved (Table 1). A variation by a factor of ten in the indium sample mass yields only a negligible deviation in the value obtained for the indium thermal resistance at zero scanning rate. Deviations of less than 10% are obtained if different aluminium pans (hand- or

Table 1

Sample thickness ( $e$ ), area ( $A$ ) and weight. Indium thermal conductivity at 372.2 K. The POM and MDPE thermal conductivities are (presumably) for the melts. The value calculated for the thermal resistance from Eq. (20) uses the tabulated thermal conductivity data. The values measured for the thermal conductivity of POM and MDPE were obtained by the procedure described in Fig. 1

	$e$ (mm)	$A$ (mm <sup>2</sup> )	Mass (mg)	$k$ (W/K m)	$R_s$ (K/W) Eq. (20)	$R_s$ (K/W)
Indium	0.20	25.03	33.157	76.20	$7.946 \times 10^{-2}$	–
POM	0.18	20.00	4.197	0.292	31.035	24.72
MDPE	0.22	33.06	5.698	0.420	15.856	10.82

press-crippled) are used. Small deformations in the bottom of the press-crippled pans may be responsible for those deviations.

The values extrapolated to zero scanning rate for POM and MDPE are 51.94 and 38.04 K/W, respectively. Following the procedure described in Fig. 1, the differences between these two thermal resistances and 27.22 K/W are the thermal resistances of POM and MDPE, respectively, at zero scanning rate (Table 1).

With the small masses used in this work, the sample thermal resistance is approximately constant for all scanning rates and consistent with the value calculated from the tabulated thermal conductivity data. The slopes of the curves (A) and (C) in Fig. 2 are similar, which indicates that, for the POM sample used, the thermal resistance varies very little with the scanning rate (POM sample mass = 4.197 mg, indium mass = 3.998 mg, hand-crippled aluminium pans). For MDPE—curve (B)—there is a small increase of the sample's thermal resistance with the scanning rate (MDPE sample mass = 5.698 mg, indium mass = 3.988 mg, press-crippled aluminium pans).

The thermal resistance may also be calculated from the thermal conductivity by

$$R_s = \frac{e}{Ak}, \quad (20)$$

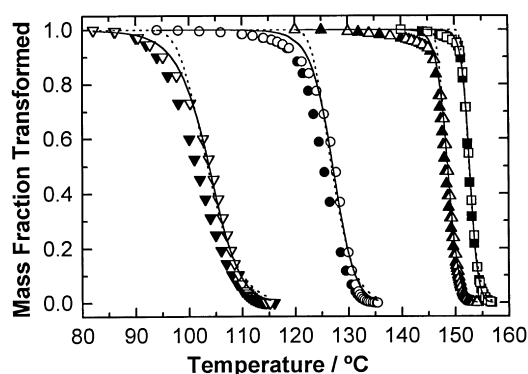


Fig. 3. Non-isothermal crystallisation of POM at scanning rates of  $-1$  ( $\square$ ),  $-5$  ( $\Delta$ ),  $-50$  ( $\circ$ ) and  $-100$  K/min ( $\nabla$ ). Full symbols are uncorrected results. Open symbols are for results corrected for the sample's thermal resistance (24.72 K/W). Sample mass = 4.328 mg. Dashed line is the fit obtained by Nakamura equation. Solid line is the fit obtained by Tobin's non-isothermal equation. The fits shown were applied over the corrected data.

where  $e$  and  $A$  are the thickness and the area of the sample, respectively, and  $k$  its thermal conductivity.

The dimensions of the samples used, their thermal conductivity, the value calculated by Eq. (20) for the sample's thermal resistance and the corresponding experimental values measured by the procedure described above are shown in Table 1. It may be seen from the data that the thermal resistance of a relatively thick indium sample is negligible when compared with the value measured from the reciprocal of the slope of its melting peak. For all curves,  $R_s$  is linearly extrapolated to zero scanning rate. The values presented in Table 1 for the thermal conductivity are for 156.6°C (the indium melting temperature); for POM and MDPE, the values were taken from the materials database of the Moldflow software package. Presumably, those values are for a temperature range in the molten state, where the thermal conductivity of the material does not change significantly. Furthermore, the values in the table are also coincident with values found in other Refs. [33,34] for the same materials but without specification of the measurement temperature.

The difference between the values calculated for the thermal conductivity and literature values is lower than that obtained in previous experiments [35] using a similar procedure. The values measured experimentally for the thermal resistances of POM and MDPE may be used to calculate their thermal conductivities at 156.6°C. Those values are 0.371 and 0.618 W/K m, respectively. The deviations between the calculated values and other published data may be attributed, apart from the errors involved in the DSC measurements, to differences between the actually measured sample masses and the values calculated from the geometrical dimensions and density, at the indium melting temperature.

#### 4.2. Non-isothermal crystallisation data

As referred to above, all cooling scans were performed with the standard DSC calibration—onset melting points of at least two high purity metal standards at the same heating rate. Since for all materials and scanning rates used the crystallisation is predominantly instantaneous, the Nakamura and Tobin equations (8) and (18), respectively, were applied in order to check for their accuracy in the description of the crystallisation

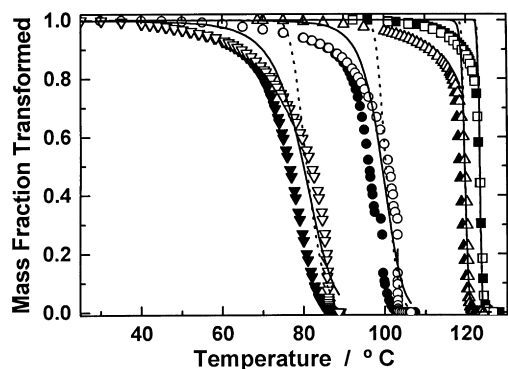


Fig. 4. Non-isothermal crystallisation of PE at scanning rates of  $-1$  ( $\square$ ),  $-5$  ( $\Delta$ ),  $-50$  ( $\circ$ ) and  $-100$  K/min ( $\nabla$ ). Full symbols are for uncorrected results. Open symbols are for results corrected for the sample thermal resistance (11.5 K/W). Sample mass = 6.078 mg. Dashed line is the fit obtained by Nakamura's equation. Solid line is the fit obtained by Tobin's non-isothermal equation. The fits shown were applied over the corrected data.

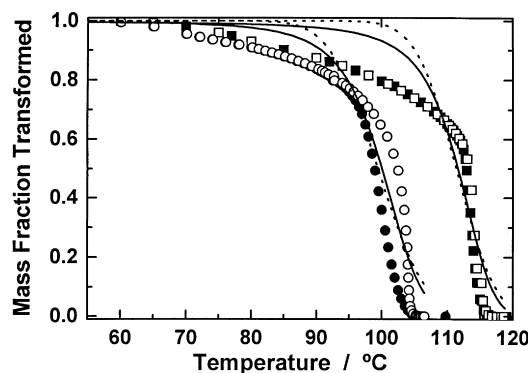


Fig. 5. Non-isothermal crystallisation of MDPE at scanning rates of  $-1$  ( $\square$ ) and  $-20$  K/min ( $\circ$ ). Full symbols are for uncorrected results. Open symbols are for results corrected for the sample's thermal resistance (23.02 K/W). Sample mass = 10.313 mg. Dashed line is the fit obtained by Nakamura's equation. Solid line is the fit obtained by Tobin's non-isothermal equation. The fits shown were applied over the corrected data.

process. These equations were applied to the non-isothermal data with and without the temperature correction for the sample's thermal resistance.

The modelling was performed using only *two parameters*: the exponent  $n$  and the overall pre-exponential factor. All other parameters were obtained from a set of isothermal experiments. The only exception made was for PEEK. Since this material crystallises very slowly, and the parameters in the transport term of the linear growth rate were not determined experimentally, they were allowed to change within reasonably narrow limits.

The data obtained for non-isothermal crystallisation of POM, PE, MDPE and PEEK are shown in Figs. 3, 4, 5 and 7, respectively. In each figure, the solid symbols represent the data as obtained from the usual calibration of the DSC (calibration on heating). Open symbols represent the data corrected for the sample's thermal resistance. Only the fits to this data are shown.

For POM (Fig. 3), and with the corrected data, values of  $n$  closer to three were obtained for both models (as expected for an instantaneous nucleation of spheres). The sum of least squares (SLS) obtained with the Tobin-type non-isothermal equation is lower, by approximately one order of magnitude,

in comparison with that obtained with the Nakamura equation (see Table 2).

Values of all parameters for PE ( $X(T)$  curves in Fig. 4), with corrected and uncorrected data, are shown for comparison in Table 3. The values of the SLS are similar for both data (corrected and uncorrected). Also for this material, Tobin's equation gives a better description of the process, which becomes more difficult for fractions of transformation greater than 80%.

The main difference between the results over the uncorrected and corrected data is that, with the latter, generally lower values for  $n$  are obtained. For MDPE and PEEK, a similar behaviour was found concerning the variation of  $n$  for corrected and uncorrected data. Also for MDPE, both types of data were modelled with Nakamura's and Tobin's equations and, as may be seen from the data in Fig. 5, the description of the process is very poor. Values for  $n$  between 1 and 2 were obtained with both equations for all scanning rates. From a physical point of view, such low values can hardly be explained. One possible cause may be linked with the microstructure formed. In fact, it has been found (see Fig. 6) that rows of columnar spherulites are formed in the middle of the solidified material, between the upper and lower columnar transcrystalline layers. Since the value

Table 2

Values of the parameters and sum of the least squares obtained with Nakamura (8) and Tobin-type (18) equations over the non-isothermal crystallisation data of POM corrected for the sample thermal resistance

dT/dt  (K/min)	Nakamura			Tobin		
	$C$ ( $\text{min}^{-1}$ ) $10^{-7}$	$n$	SLS $\times 10$	$C$ ( $\text{min}^{-1}$ ) $\times 10^{-7}$	$n$	SLS $\times 100$
1	181.41	2.51	0.5	187.95	3.56	0.9
5	211.59	2.41	0.6	217.51	3.08	1.9
10	127.60	2.45	0.8	129.86	3.08	3.6
20	82.64	2.13	2.1	86.64	2.89	7.6
50	3.92	2.42	1.5	16.22	3.19	5.2
100	3.22	3.15	1.1	2.33	4.16	2.5

Table 3

Parameter values obtained with Tobin's non-isothermal equation for corrected and uncorrected PE data. The sum of the least squares obtained for each case is also shown. The sample's thermal resistance used for correcting the data was constant and equal to 11.5 K/W

dT/dt  (K/min)	Uncorrected data			Corrected data		
	$C \text{ (min}^{-1}) \times 10^{-3}$	$n$	SLS $\times 10$	$C \text{ (min}^{-1}) \times 10^{-5}$	$n$	SLS $\times 10$
1	9.89	3.4	1.3	1029	2.9	2.8
5	9.35	3.6	1.5	87	3.0	3.6
10	7.52	3.8	1.7	36	3.1	5.3
20	5.10	3.7	2.2	10	2.5	6.9
50	3.92	5.8	0.6	26	2.6	5.3
100	3.22	9.3	0.3	6.3	4.4	3.7

found for  $n$  is an average for the geometry of all crystalline structures present within the sample, the low dimensionality of the columnar spherulites may well contribute to the low values measured. In addition, another possible cause is that a DSC calibration on cooling (rather than on heating) should have been used in the experiments or in the data treatment procedures. This important and difficult problem is, at present, the subject of much research interest and will be discussed in a separate report [27].

Concerning the non-isothermal crystallisation of PEEK (Fig. 7), and since this is a slowly crystallising material, and the activation energy for transport was not calculated from the experimental data, two additional parameters were allowed to change ( $C_1$  and  $C_2$ ). Average values obtained for  $C_1$  and  $C_2$  are 18 and 111, respectively. Apart the lowest cooling rate, and with the exception of the last 10% of the transformation process, the description of the process may be considered as reasonable. However, a physical meaning can hardly be found for the parameters obtained with this description. Concerning the variation of  $n$ , the opposite behaviour to that found for MDPE was found for PEEK. Here,  $n$  changes from 2.61 at  $-5$  K/min to 9.4 at  $-100$  K/min (higher values are obtained when uncorrected data are

used). Such values are also unacceptable from a physical point of view. Optical microscopy experiments, performed on the same material as the one used in these experiments, show that the crystalline structures have a spherical shape and that the nucleation is heterogeneous. Values of  $n$  near to 3 are thus expected. The reason for such unexpected behaviour also seems to be linked to the need for a proper DSC calibration on cooling. In fact, it was recently found that when this calibration is carried out, the values obtained for  $n$  are close to the expected ones [17,27], as a result of significant temperature shifts relative to the temperatures measured with the conventional calibration (e.g. 5 K for a cooling rate of 10 K/min [16] and 30 K for a cooling rate of 100 K/min). Also, better descriptions of the crystallisation process can, generally, be achieved, as well as a more consistent variation of the pre-exponential factor with the cooling rate.

#### 4.3. Non-isothermal modelling of isothermal crystallisation data

Considering the contribution of the sample's thermal resistance and of the heat released during crystallisation,

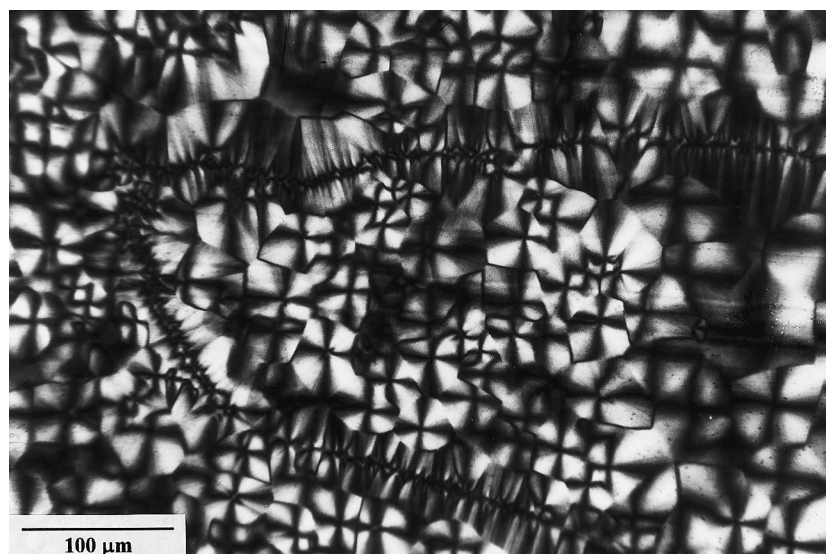


Fig. 6. Section of a MDPE sample as shown by polarised optical microscopy. Sample crystallised in a DSC at a scanning rate of  $-20$  K/min.

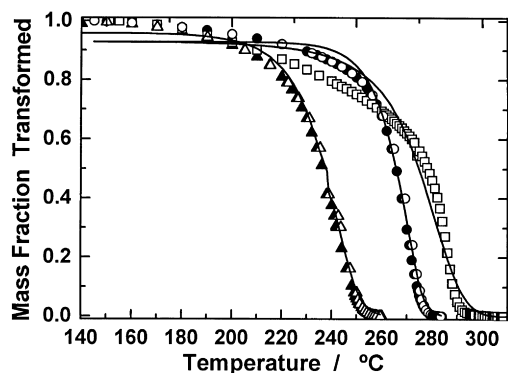


Fig. 7. Non-isothermal crystallisation of PEEK at scanning rates of  $-5$  ( $\square$ ),  $-50$  ( $\circ$ ) and  $-100$  K/min ( $\triangle$ ). Full symbols are for uncorrected results. Open symbols are for results corrected for the sample's thermal resistance (32.45 K/W). Sample mass = 9.987 mg. Solid line is the fit obtained by Tobin's non-isothermal equation applied over the corrected data.

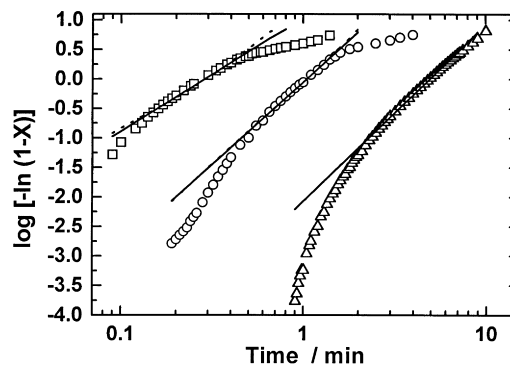


Fig. 8. Isothermal crystallisation of POM at temperatures  $149^{\circ}\text{C}$  ( $\square$ ),  $153^{\circ}\text{C}$  ( $\circ$ ) and  $157^{\circ}\text{C}$  ( $\triangle$ ). Symbols are for experimental data. The solid line shows the modelling results obtained with Avrami's equation. The dotted line represents results obtained with Nakamura's equation (applied after accounting for the sample's temperature variation during crystallisation).

the true sample temperature in an isothermal experiment may be calculated from Eq. (19). The calculations, performed over results of isothermal crystallisation of POM, yielded the sample temperature increase during each experiment, as a function of time [17]. In this way, an isothermal process may, and indeed should, be considered as truly non-isothermal and treated as such.

As an additional test of the modelling procedure presented here, namely the use of isothermal data to model non-isothermal experiments [17], Nakamura's and Tobin's equations were applied to isothermal data, where time was substituted by the actual sample temperature during the experiment. The results of this exercise are shown for three crystallisation temperatures in Fig. 8 and Table 4. In Fig. 8, the modelling of data obtained with Avrami's equation for isothermal crystallisation is compared with the modelling obtained with Nakamura's equation for non-isothermal crystallisation. If Tobin's equation is applied, a similar behaviour is obtained for the variation of the parameters obtained with the two approaches, although a better fit to the experimental data is achieved.

As expected, for lower crystallisation temperatures, where the sample temperature increase is much more pronounced ( $\approx 2$  K), the differences between the fits obtained with the two approaches (Avrami's and Nakamura's) are greater. For higher crystallisation temperatures,

the sample temperature increase is small ( $\approx 0.2$  K), and identical results are obtained with the two approaches. The equivalence of the two procedures can be checked through the data of Table 4.

### 5. Conclusions

It is not physically reasonable to arbitrarily change the parameters of the Nakamura or Tobin equations to fit non-isothermal crystallisation kinetics. It was shown, by polarised optical microscopy, that the parameters of the linear growth rate expression (namely  $K_g$ ) are the same—within experimental errors—for isothermal and non-isothermal experiments [36]. Physically, there is in fact no reason why it should not be so. Following the reasoning used to derive the Nakamura and Tobin equations for instantaneous nucleation, the parameters obtained from isothermal experiments must be valid to describe non-isothermal ones.

The procedure used here to correct non-isothermal crystallisation data (obtained with the calibration on heating) for the sample's thermal resistance is as previously reported in the literature [14], but the resistance is calculated in a different way. However, large deviations in the temperature scale, especially critical at high cooling rates, cannot be fully accounted for by the above procedure, unless a proper calibration on cooling is performed, followed by the correction for the thermal resistance. This may well be one of the reasons for the failure of the modelling process. Another may be related with the equations used as, for some cooling rates, the nucleation is of the mixed type (instantaneous and sporadic). In addition, as it happens in isothermal experiments, two stage crystallisation processes may occur and more complex equations are then needed. These problems will be addressed in future reports.

Table 4  
Kinetic parameters and Avrami's exponents obtained for the isothermal crystallisation of POM at the indicated temperatures, with Avrami's and Nakamura's equations

T (°C)	Avrami		Nakamura/Avrami	
	K (s <sup>-n</sup> )	n	K (s <sup>-n</sup> )	n
149	$4.72 \times 10^{-3}$	1.93	$1.99 \times 10^{-2}$	2.11
153	$8.90 \times 10^{-6}$	2.78	$9.54 \times 10^{-5}$	2.91
157	$4.16 \times 10^{-8}$	2.98	$6.58 \times 10^{-7}$	3.02

**References**

- [1] Phillips R, Manson J-AE. *J Polym Sci B: Polym Phys* 1997; 35:875.
- [2] Wasiak A. *Chemtracts Macromol Chem* 1991;2:211.
- [3] Patel RM, Spruiell JE. *Polym Engng & Sci* 1991;31:730.
- [4] Nakamura K, Watanabe T, Katayama K, Amano T. *J Appl Polym Sci* 1972;16:1077.
- [5] Nakamura K, Katayama K, Amano T. *J Appl Polym Sci* 1973;17:1031.
- [6] Nakamura K, Watanabe T, Amano T, Katayama K. *J Appl Polym Sci* 1974;18:615.
- [7] Ozawa T. *Polymer* 1971;12:150.
- [8] Kolmogoroff AN. *Izvest Akad Nauk SSR, Ser Math* 1937;1:335.
- [9] Avrami M. *J Chem Phys* 1939;7:1103.
- [10] Avrami M. *J Chem Phys* 1940;8:212.
- [11] Avrami M. *J Chem Phys* 1941;9:177.
- [12] Evans UR. *Trans Faraday Soc* 1945;41:365.
- [13] Martins JA, Cruz-Pinto JJC. *J Thermal Anal* 1993;40:621.
- [14] Chan TW, Isayev AI. *Polym Engng Sci* 1994;34:461.
- [15] Hammami A, Spruiell JE. *Polym Engng Sci* 1995;35:797.
- [16] Martins JA, Cruz-Pinto JJC. *Thermochim. Acta* 1999;332:17.
- [17] Martins JA. *Cristalização de Polímeros: estudo experimental e modelação teórica*. PhD Thesis, Universidade do Minho, 1996.
- [18] Wunderlich B. *Macromolecular physics*, Vol. 2. New York: Academic Press, 1976.
- [19] Martins JA, Cruz-Pinto JJC. In preparation.
- [20] Miller RL, editor. *Flow induced crystallization in polymer systems* London: Gordon and Breach, 1977.
- [21] Tobin MC. *J Polym Sci, Polym Phys Ed* 1974;12:399.
- [22] Tobin MC. *J Polym Sci, Polym Phys Ed* 1976;14:2253.
- [23] Cruz-Pinto JJC, Martins JA, Oliveira MJ. *Colloid Polym Sci* 1994;272:1.
- [24] Cruz-Pinto JJC. In preparation.
- [25] Cruz-Pinto JJC, Martins JA. Modelling the isothermal crystallization of engineering polymers. In: Dosièrè M, editor. *Crystallization of polymers*, NATO ASI Series on Mathematical and Physical Sciences-Dordrecht: Kluwer Academic, 1993.
- [26] Patel RM, Spruiell JE. *Polym Engng Sci* 1991;31:730.
- [27] Martins JA, Cruz-Pinto JJC. In preparation.
- [28] Janeschitz-Kriegl H, Wippel H, Paulik C, Eder G. *Colloid Polym Sci* 1993;271:1107.
- [29] Hoffman JD. *Polymer* 1983;24:3.
- [30] Cebe P, Hong SD. *Polym Engng Sci* 1984;27:1183.
- [31] Bershtein VA, Egorov VM. *Differential scanning calorimetry of polymers*, Ellis Horwood Series in Polymer Science and Technology. Chichester, UK: Ellis Horwood, 1994.
- [32] Richardson MJ. *Thermochim Acta* 1997;300:15.
- [33] Brandup J, Immergut EH, editors. *Polymer handbook* 3rd ed.. New York: Wiley, 1989.
- [34] Mark JE, editor. *Physical properties of polymers handbook* American Institute of Physics, 1996.
- [35] Flynn JH, Levin DM. *Thermochim Acta* 1988;126:93.
- [36] Martins JA, Cruz-Pinto JJC. *J Thermal Anal* 1993;40:629.